Chapter 2 - Quantifying the effect of root hair architecture on wheat physiology

Ian Tsang

October 2024

1 Introduction

Root hairs are single cell projections that extend from the surface of the root, and are critical for nutrient and water uptake (Tsang et al. 2024). Optimization of root hair architecture is likely key to maximize crop performance in the field (Tsang et al. 2024). Increasing root hair length and density in modern crops will likely improve nitrogen, phosphorous, water uptake and grain yield (Gahoonia et al. 1998, Saengwilai et al. 2021). As we manouver towards an era of lower input agriculture, root hairs will likely play an increasingly large role in maintaining crop health and productivity in the field.

1.1 Nitrogen

Nitrogen (N) is the the most critical soil nutrient for plants, as it serves as a key element in many metabolites. The 'plastic' nature of plant root systems enable them to adapt to foraging for N in soil, which is critical for N uptake (Bienert et al. 2021). In soil, N primarily exists in the form of inorganic ions: nitrate (NO_3^-) and ammonium (NH_4^+), where ammonium is more prominant in water logged, acidic soils (Bienert et al. 2021).

Root hair morphology is plastic in response to N availability. For example, in *Arabidopsis*, increasing nitrate concentration increases root hair density (RHD) via reducing the length of trichoblasts, resulting in an increased number of trichoblasts per unit of root (Canales et al. 2017). A lack of root hairs in the *rhd6-3* mutant resulted in decreased root nitrate concentration in contrast with the wild-type (Canales et al. 2017). Conversely, high ammonium concentrations reduced root hair elongation, but increased root hair branching in *Arabidopsis*, where the increased branching phenotype was due to altered cytoplasmic streaming in root hair tips (Yang et al. 2011). Since ammonium is toxic to plants in large quantities, the reduction in root hair elongation is likely an adaptation to reduce ammonium uptake. However, since ammonium uptake requires less energy for assimilation in contrast to nitrates, it may be the preferred source of N for N uptake in *Arabidopsis* (Ludewig et al. 2002). In other species, root hairs also play a critical role in N uptake. Simulation results from (Saengwilai et al. 2021) revealed that longer, denser root hairs were predicted to improve N acquisition in maize. In the field, maize varieties with longer root hairs experienced increased plant biomass, N content and yield relative to varieties with shorter root hairs (Saengwilai et al. 2021). Nitrogen starvation in cotton (*Gossypium hirsutum L.*) increased both root hair length and density (Zhu et al. 2022). Similar results from (Foehse et al. 1983) revealed that N deficiency stimulated longer root hair

development in tomato, spinach and oilseed rape. Taken together, these results highlight the function and importance of root hairs in N acquisition, and the plastic nature of roots and root hairs in response to N availability in the environment.

1.2 Phosphorus

Phosphate (P) is another critical soil element that is required by plants, but is often less available due to the lack of mobility in soil (Bienert et al. 2021). Similar to N, root hairs are key for P uptake from soil, with root hair morphology strongly affecting P uptake rates. As P mobility in soil is governed by diffusion rather than mass flow, P uptake in plants is often limited to a region of the local rhizosphere (Barber et al. 1963). Thus, longer root hairs extends the depletion zone boundary around plant roots, increasing the amount of P accessible to the plant (Bienert et al. 2021). In the commmon bean *Phaseolus vulgaris*, varieties with longer root hairs and short roots experienced the largest increase in plant biomass under P deficiency in contrast to varieties with other root architetures (Miguel et al. 2015). Similarly, maize lines with longer root hairs exhibited increased plant growth, P uptake and P absorption rate in contrast to lines with shorter root hairs (Zhu et al. 2010). The bald root barley (*brb*) mutant exhibited half as much P uptake compared to the wild-type with longer root hairs, where the wild-type displayed a more uniform P depletion zone surrounding the root compared to the *brb* mutant (Gahoonia et al. 2004). Taken together, these results highlight the importance of root hairs for P uptake.

1.3 Water Uptake

While the role of root hairs in nutrient uptake is well characterized across different species, its role in water uptake is disputed. In wet soils, water flow is primarily governed by roots, whereas in dry soils, root hairs likely play a more active role in water uptake by increasing the root radius (Cai et al. 2022). In barley, the *brb* mutant displayed higher xylem suction in contrast to the wild-type with longer root hairs (Carminati et al. 2017). The authors concluded that root hairs aid water uptake by reducing the decrease in matric potential (the portion of water potential that can be attributed to the attraction of the soil matrix towards water (Kirkham 2014)) betwen the root and soil during transpiration. Marin et al. 2021 revealed that under field conditions, root hairs positively contributed to plant water status and stress tolerance under drought conditions by reducing negative leaf water potential, abscisic acid (ABA) accumulation in the leaf, and increasing shoot P accumulation. In addition, root hairs enhanced yield stability under drought conditions in barley genotypes with longer root hairs compared to shorter hairs (Marin et al. 2021).

However, in contrasting studies, Dodd et al. 2016 found that the *brb* mutant maintained similar shoot growth and transpiration rates compared to the wild-type under drought conditions at varying P concentrations, implying root hairs play a minor role in water uptake during drought. Similarly, Cai et al. 2021 reported that the maize *roothairless3 (rth3)* mutant (Hochholdinger et al. 2008) did not differ in leaf xylem water potential compared to the wild-type during soil drying, suggesting root hairs in maize likely play a minor contribution to water uptake during drought stress.

1.4 Hyperspectral Reflectance

To quantify the effect of root hair morphology on plant physiology, various techniques can be deployed. Traditional plant physiology measurements involve harvesting plants at maturity and recording biomass traits such as plant height or tiller number. However, methods such as this are labour intensive and subject to sampling and measurement bias. More complex techniques, including utilization of automation and technical equipment is likely to provide higher quality data with an increased throughput.

Hyperspectral reflectance measurements are fast and non-invasive, enabling the screening of many physiology traits from measuring leaf reflectance (Silva-Perez et al. 2018). Traditionally, capturing more complex traits (such as gas exchange or leaf mass area (LMA)) are time consuming and destructive, unsuitable for high throughput, repetitive screening of germplasm (Furbank et al. 2021). Conversely, hyperspectral measurements are quick and easy to conduct. In contrast to traditional spectral photometers, hyperspectral machines can detect the full wavelength spectrum (300-2500nm) and are thus able to harness information from the infrared (IR) regions to measure a wide array of traits (Silva-Perez et al. 2018). From the visible (VIS) and near-infrared (NIR) regions of the spectrum, the ratio of red to infrared has been used to infer chlorophyll content in leaves (Datt 1999). The indices NDVI (normalized difference vegatative index) - a measure of vegetation greenes and foliage development, and NDWI (normalized vegetative water contnet) are both calculated from leaf reflectance in the VIS and NIR regions (Gutierrez et al. 2010, Montesinos-López et al. 2017). V_{cmax} - a measure of maximum RuBisCo carboxylation, and J - a measure of electron transport during photosynthesis have both been accurately estimated from leaf reflectance measurements (Ainsworth et al. 2014). In wheat, reflectance from the IR regions have been used to predict grain yield (Montesinos-López et al. 2017) and leaf nitrogen content (Yao et al. 2015). Furthermore, using hyperspectral reflctance to estimate plant physiological traits has been applied to many different plant species, including maize (Yendrek et al. 2017), rice (Das et al. 2020), soybean (Ainsworth et al. 2014) and mango (Mahajan et al. 2021). Numerous machine learning (ML) approaches have been adopted to predict physiology traits from leaf hyperspectral measurements, including wheat physiology predictor that accurately predicts 10 different physiology traits (Furbank et al. 2021).

1.5 Field Physiology

In contrast to previous sections, very few studies have quantified how root hair morphology influences crop physiology in the field. As perviously described, Marin et al. 2021 showed that root hairs contributed to yield stability in barley under drought conditions. Gahoonia et al. 2004 previously demonstrated that barley genotypes with longer root hairs improve grain yield under low soil P conditions. The maize *rth3* mutant exhibited significantly lower grain yield compared to the wild-type across three separate trials (Hochholdinger et al. 2008). Across a range of spring wheat cultivars, root hair length (RHL) was positively correlated with biomass and grain yield in both drought and well-watered conditions (Maqbool et al. 2022). While these few studies begin to demonstrate the impact of root hair morphology on crop physiology, none have been focused on wheat (*Triticum aestivum L.*), the UK's most produced crop.

Here, we report the first known study quantifying the effects of root hair morphology on bread wheat physiology. We utilize an array of phenotyping techniques, including hyperspectral reflectance, automated

plot scanning and isotopic analysis to determine physiological differences between the root hair mutant *srh1* and wild-type.

2 Materials and Methods

2.1 Field Trials

2.1.1 Nursery Trials

For in depth evaluation of the physiological differences between the root hair wild-type and *srh1* mutant, nursery trials were conducted in Cambridgeshire across three consecutive years. For all subsequent trials, seeds were sourced from purity plants (single plant descent). Trial designs for all three years were carried out using a randomized block design across 2 blocks (Table 1). Each trial contained 5 WT and 5 *srh1* plots derived from a different individual parental backcross. Each one of these plots was replicated between the two blocks (Block 1: Plots 1-10, Block 2: Plots 11-20, Table 1). Across all three years, plots were treated with pre-emergence and standard herbicides, as well as nutrient fertilizers. The 2023 and 2024 trials were located in Hinxton (52.091475, 0.175449) South Cambridgeshire, UK, while the 2025 nursery trial was located on the NIAB trial site (52.243168, 0.103581).

2.1.2 Yield Trials

To establish the impact of root hair morphology on wheat yield, yield trials were conducted in 2024 and 2025. For each year, two yield trial sites were established. In 2024, yield trials were located in Hinxton, South Cambridgeshire (52.099238, 0.175695) and Morley, Norfolk (52.559640, 1.041967) and located in Duxford () and Cambridge (52.243334, 0.104070) in 2025. Each trial site comprised 20 plots of the *srh1* mutant and wild-type in a complete randomized block design. Each trial utilized bulked seed stocks from the previous year's nursery trials. For each trial, seeds were sown at a population target of 250 plants/m^2 with an estimated germination and survival rate of 90%. The per-plot seed weight was estimated from the thousand grain weight (TGW). All plots were 6m x 2m and each trial was arranged in a 4 x 5 grid (Table 2). An imbalanced trial design was implemented in Morley in 2024 due to a lack of sufficient seed for *srh1* plots.

2.2 Field Trial Phenotyping

2.2.1 Above ground physiology

In the 2023 nursery trial, 12 plants were randomly sampled from each plot. Traits including tiller height, internode distances, ear length, weight, and spikelet number were collected from these plants. Grain properties (e.g. TGW, size, area) were collected from oven dried ears and measured using a MARViN ProLine (MARViTECH, GmbH, Germany).

An identical sampling strategy was deployed in subsequent nursery trials in 2024 and 2025. Only plant height, ear length and grain dimensions were recorded. All other traits previously recorded in 2023 exhibited no obvious differences, and were excluded for ease of measurement.

Plot	2023	2024	2025
1	WT	MUT	WT
2	MUT	MUT	MUT
3	MUT	WT	WT
4	WT	MUT	MUT
5	MUT	WT	WT
6	MUT	WT	MUT
7	WT	WT	MUT
8	MUT	MUT	WT
9	WT	MUT	MUT
10	WT	WT	WT
11	WT	MUT	WT
12	MUT	WT	MUT
13	MUT	MUT	WT
14	MUT	MUT	WT
15	WT	WT	MUT
16	WT	MUT	WT
17	MUT	WT	WT
18	WT	MUT	MUT
19	MUT	WT	MUT
20	WT	WT	MUT

Table 1: Table illustrating randomized block design of the spring nursery trial design across three consecutive years. 2024 and 2025 trials were supplied by single purity plant descent from 2023 and 2024 respectively. Connecting arrows (red: MUT, green: WT) illustrate purity plant descent between plots across years. Generations: 2023 - BC_2F_4, 2024 - BC_2F_5, 2025 - BC_2F_6. WT: root hair wild-type, MUT: root hair mutant *srh1*.

Hinxton 2024			
MUT	WT	MUT	WT
WT	MUT	WT	MUT
MUT	WT	MUT	WT
WT	WT	WT	MUT
WT	MUT	WT	WT

Cambridge 2025			
WT	MUT	MUT	MUT
MUT	MUT	MUT	WT
MUT	WT	WT	WT
WT	MUT	MUT	WT
WT	WT	WT	MUT

Morley 2024			
WT	MUT	WT	WT
WT	WT	MUT	WT
WT	MUT	WT	WT
WT	MUT	MUT	WT
MUT	WT	WT	MUT

Duxford 2025			
MUT	WT	WT	MUT
MUT	WT	MUT	MUT
WT*	MUT*	MUT*	WT*
MUT	WT	WT	WT
MUT*	WT*	WT	MUT

Table 2: Yield trial designs in 2024 and 2025 across the four locations. *s indicate plots with errors during the drilling process.

2.2.2 Below ground physiology

From the 2023 nursery, 12 whole plant root samples were collected from each plot via shovelomics (Fradgley et al. 2020). Root samples were soaked in warm water with fairy liquid for 5 minutes, and gently massaged under running water to remove the soil. The exposed roots were then thoroughly dried using a hair dryer, and stored at 4°C. Dried root samples were then placed on black card along the plane with the most number of crown roots. Each sample was imaged from above using an Olympus E-M1 Mark II camera attached to a camera stand, flipped 180°, and imaged again. Crown root number (CRN), nodal root number (NRN) and seminal root number (SRN) were visually scored, while crown root angle (CRA) was calculated from the acquired images. For each root sample, CRA was calculated as the mean angle between the widest available pair of crown roots between images captured across the two planes.

2.3 Isotope Discrimination

2.3.1 Leaf Disc Sampling

Flag leaf discs were sampled from the 2024 nursery trial on 27/6/2024. Samples were collected using a standard circular leaf bore, with three leaf discs taken per plant. Discs were collected from the same plant that had its roots harvested for AMF. The leaf discs were stored in labelled tubes for each plot, and the tubes were left to dry in an oven at 65°C for four days with the lids open. After four days, the samples were sealed in the tubes.

2.3.2 Isotope Measurements

Leaf Nitrogen %, Carbon %, δ15N and δ13C analysis was carried out at The Godwin Laboratory for Palaeoclimate Research, Department of Earth Sciences, University of Cambridge, Downing Street, Cambridge, CB2 3EQ, UK. Analysis was carried out using a Costech Elemental Analyser coupled with a Thermo DELTA V mass spectrometer via a Conflo IV in continuous flow mode. Leaf samples were analysed for percentage carbon, percentage nitrogen, δ13C and δ15N isotope ratios.

Dried samples were weighed, placed into tin capsules, sealed, and loaded into the sampler. Samples were flash-combusted in the reactor at 1500°C in an oxygen-enriched atmosphere. Result elemental components were carried by helium through an oxidation catalyst comprising chromium trioxide and silver-coated cobaltic oxide at 1020°C. Excess oxygen was removed in a reduction tube with metallic coper at 650°C. Water vapour was removed using magnesium perchlorate, and the gases were separated in a gas chromatographic column at 45°C.

The separated gases were measured by the mass spectrometer. Area under the peak for Nitrogen and CO_2 were sed to determine the percentage of Nitrogen and Carbon respectively. δ13C and δ15N isotope ratios were directly measured by the spectrometer. At the start of the run, weighted standards were analysed to calculate percentage Nitrogen and Carbon for the batch. Results were calibrated to reference standards from the International Atomic Energy Agency (IAEA). Precision of analyses was $\pm$0.5% for Carbon/Nitrogen abundance, ¿0.1‰ for δ13C and δ15C.

2.4 Spectral Reflectance

2.4.1 Measurements

To efficiently estimate photosynthetic differences between the *srh1* and wild-type in the field, hyperspectral reflectance measurements were carried out in 2024 and 2025 on the nursery trials. Reflectance measurements were carried out using an ASD FieldSpec 4 (FS4) (Malvern Panalytical, USA) in 2024, and a PSR +3500 with a reflectance sphere attachment (NERC) in 2025. The ASD FS4 spectrometer had a sampling interval of $1nm$ with a spectral range between 350-2500nm, and was equipped with three detectors: Visible and Near Infra-Red (VNIR): 350-1000nm; Short Wave Infra-Red (SWIR) 1: 1000-1800nm; SWRI 2: 1800-2500nm.

Measurements were conducted on the 2024 nursery trial at 5 different time points across the growing season (27/6/24, 4/7/24, 11/7/24, 18/7/24, 30/7/24 and 7/8/2024) (Table 3). All measurements were taken on relatively sunny days with low/no cloud cover between 0800 and 1100. The ASD FieldSpec4 was connected to a laptop with the ASD ViewSpecPro 3 Software for data acquisition.

Date of sampling	Description	Growth Stage
27/6/2024	Start of ear emergence	GS 51-55
4/7/2024	50% ear emergence	GS 55
11/7/2024	$\sim$ 100% ear emergence	GS 59
18/7/2024	Flowering/Anthesis	GS 61-65
30/7/2024	Grain forming	GS 71-73
7/8/2024	Dough development	GS 83-85

Table 3: Description of growth stages during different Field Spec measurement timepoints. Growth Stages according to Zadoks scale

To operate the spectral reflectance devices, the light source was first warmed up for 10 minutes. White reference calibration measurements taken against a white background after each plot. Leaf measurements were performed against a black background. A 3-D printed black cuvette was positioned on top of the light source to standardize the area of light directed onto each leaf. White reference measurements were performed with the cuvette attached. Measurements were taken from the adaxial side of leaves, close to where the leaf attaches to the stem. Three technical replicates were performed on each leaf, and five different leaves from five different plants were measured in each plot. Where possible, plants with healthy leaves were selected, avoiding diseased/yellowing/patchy leaves.

2.4.2 Cuvette

The cuvettes for the ASD FS4 and PSR+ 3500 were created using the CAD modelling software OpenSCAD (`https://openscad.org/`). For the FS4 cuvette, the mask had an outer diameter of 32.3mm; an inner cut-out diameter 27.4mm, with the leaf cutout window of 18.8mm x 6mm. The PSR+3500 cuvette had an outer diameter of 55mm, an inner cut-out diameter of 51.3mm, and a 22mm x 7mm leaf cutout window.

The raw CAD files were sliced with the 3-D printing software Ultimaker Cura, which generated an STL(Standard Tesselation Language) file. The cuvettes were printed from the STL files using an Ultimaker S3 3-D printer, with an AA 0.4mmprint core using Tough Black Polylactic Acid (PLA) as the print

material.

2.4.3 Physiology Trait Prediction

ASD files were used to store the recorded spectral reflectance measurements from the ASD FS4. The R package 'asdreader' (`10.32614/CRAN.package.asdreader`) was used to convert the binary values in .ASD files into numerical values. Output SED files from the PSR+3500 were parsed using a custom python script. For both sets of measurements, replicates displaying anomalous spectra were removed. Photosynthetic traits were subsequently predicted using wheat physiology predictor (`https://wheatpredictor.appf.org.au/`, Furbank et al. 2021) with the 'Ensemble' model. Jumps were set at 1000 and 1800 for ASD FS4.

2.5 Field Scanalyzer

2.5.1 Trial Design 2024

As part of the PhenomUK Access to Facilities Grant (41555058) that I was awarded, nursery trials of the *srh1* and wild-type were grown at Rothamstead Research (51.806467, -0.361601) in 2024 and 2025. The objective of this project was to perform detailed time-course measurements of above ground physiology of the *srh1* mutant and wild-type.

Seeds used for the initial trial in 2024 were sourced from leftover seeds from the 2023 spring nursery. Seeds harvested from this trial in 2024 were used to populate the 2025 trial. The trial design in 2024 comprised 16 total plots, with eight *srh1* mutant and eight wild-type plots, drilled across 2 blocks in a complete ranomized block design. Six plots of each genotype were from the BC_2F_4 generation, while the remaining 2 plots per genotype were BC_2F_4. The trial design in 2025 comprised 12 plots (6 wild-type, 6 *srh1*). All plots in the 2025 trial (BC_2F_5) were sourced from seeds from the BC_2F_4 plots in the 2024 trial.

361-MUT-F3	—	369-WT-F3
362-WT-F3	—	370-MUT-F2
363-MUT-F3	—	371-WT-F3
364-WT-F3	—	372-MUT-F3
365-WT-F2	—	373-MUT-F3
366-WT-F3	—	374-MUT-F3
376-MUT-F2	—	375-WT-F3
368-MUT-F3	—	376-WT-F2

Table 4: RRes trial layout 2024

2.5.2 Scanner Sensors

The field scanalyzer was equipped with 2 3D laser scanners and RGB cameras. The 3D laser scanners (Fraunhofer Instituite, Munich, Germany) utilized a near infrared (NIR) laser ($840nm$) to scan each plot canopy in the x-y-z axis, with an field-of-view (FOV) of 0.5m x 0.5m. Point cloud images were generated for each plot, enabling quantification of plant height at a throughput of approximately 30 plots per hour. The RGB cameras on the platform (Allied Vision, Stadtroda, Germany) captured high resolution images (3296 x 2472px) in 12 colour bit. The cameras were set up perpendicular to the ground, capturing approximately

180 images per hour. Fraction vegetation cover (FVC) was calculated from the RGB images as a ratio of the total number of green pixels divided by the total number of pixels for a given area, while plant height was extracted from the 3D point clouds via a segmentation algorithm. For plant height calculation, each plot was divided into 12 quadrants, and the plant height was calculated for each quadrant in each plot. Mean plot plant height was thus calculated as average across the 12 regions. Growth rates of plant height and FVC were calculated as growth rate per day by dividing the change in plant height/FVC between the number of elapsed days between each timepoint. The scanner was in operation from 21/5/24-14/8/24, capturing canopy scans across 9 time points and RGB images across 17 time points.

2.6 Statistical Testing

The R package r/lme4 was used to fit generalized linear mixed-effect models on all datasets presented in this chapter. For all datasets, the primary objective was to determine the effect of genotype (*srh1* versus wild-type) against a particular trait. The following models were used for the following datasets:

$$\text{Plant Height: } \text{lmer}\left(\text{Plant Height} \sim \text{Year} * \text{Genotype} + (1 \mid \text{Plot}) + (1 \mid \text{Block})\right) \tag{1}$$

$$\text{Spike Length: } \text{lmer}\left(\text{Spike Length} \sim \text{Year} + \text{Genotype} + \text{Block} + (1 \mid \text{Plot})\right) \tag{2}$$

$$\text{TGW/Grain Dimensions: } \text{lmer}\left(\text{TGW/Grain} \sim \text{Year} * \text{Genotype} + (1 \mid \text{Block})\right) \tag{3}$$

$$\text{Isotope: } \text{lmer}\left(\text{Isotope} \sim (1 \mid \text{Plot}) + \text{Rep} + \text{Genotype}\right) \tag{4}$$

$$\text{Physiology Prediction: } \text{lmer}\left(\text{Trait} \sim (1 \mid \text{Plot}) + \text{Genotype} * \text{Timepoint}\right) \tag{5}$$

$$\text{Scanner Height and FVC: } \text{lmer}\left(\text{Trait} \sim (1 \mid \text{Plot}) + (1 \mid \text{Block}) + \text{Generation} + \text{Timepoint} + \text{Genotype}\right) \tag{6}$$

The random effects 'Plot' and 'Block' did not contribute any variance to the height and fvc growth rates of the *srh1* mutant and wild-type, and were thus removed from the model. A simple linear model was used instead:

$$\text{Growth Rates: } \text{lm}\left(\text{Trait} \sim \text{Generation} + \text{Genotype} * \text{Timepoint}\right) \tag{7}$$

2.7 Data Visualization

All data visualization was carried out using the python (v3.12.5) libraries matplotlib (Hunter 2007) and seaborn.

3 Results

Trait	Description	Unit	Data Acquisition
LMA	Dry leaf mass area	$g\ m^{-2}$	ASD Field Spec 4
N_{area}	Leaf nitrogen per unit area	$g\ N\ m^{-2}$	ASD Field Spec 4
N_{mass}	Leaf nitrogen concentration	$mg\ N\ g^{-1}$	ASD Field Spec 4
J	Rate of electron transport during photosynthesis	$\mu mol\ e^{-}\ m^{-2}\ s^{-1}$	ASD Field Spec 4
V_{cmax}	Maximum velocity of Rubisco carboxylation	$\mu mol\ CO_2\ m^{-2}\ s^{-1}$	ASD Field Spec 4
V_{cmax25}	Maximum velocity of Rubisco carboxylation normalized to 25°C	$\mu mol\ CO_2\ m^{-2}\ s^{-1}$	ASD Field Spec 4
V_{cmax25}/N_{area}	Maximum velocity of Rubisco carboxylation (25°C) per unit area of leaf nitrogen	$\mu mol\ CO_2\ s^{-1}\ (g\ N^{-1})$	ASD Field Spec 4
Cond	Stomatal conductance	$mol\ H_2O\ m^{-2}\ s^{-1}$	ASD Field Spec 4
SPAD	Surrogate for chlorophyll content	-	ASD Field Spec 4
Photo	CO2 assimilation rate	$\mu mol\ CO_2\ m^{-2}\ s^{-1}$	ASD Field Spec 4
Plant Height	Measured from base of roots to the end of the spike on the tallest tiller	cm	Field Scanner (Laser scanner) and manual measurement
FVC	Fraction vegetation cover, a ratio of green pixels to overall pixels	-	Field Scanner (RGB Cameras)
TGW	Thousand grain weight	g	MARViN ProLine
Area	Grain area	mm^2	MARViN ProLine
Length	Grain length	mm	MARViN ProLine
Width	Grain width	mm	MARViN ProLine
Spike length	Length of the spike/ear from top to bottom	cm	Manual measurement
Carbon %	Percentage of Carbon in dry leaf matter	-	Mass spectrometry and elemental analyzer
Nitrogen %	Percentage of Nitrogen in dry leaf matter	-	Mass spectrometry and elemental analyzer
δ13C	Ratio of Carbon 13 to Carbon 12 isotopes in dry leaf matter	-	Mass spectrometry and elemental analyzer
δ15N	Ratio of Nitrogen 15 to Nitrogen 14 isotopes in dry leaf matter	-	Mass spectrometry and elemental analyzer

Table 5: Description of all measured physiological traits from the *srh1* mutant and wild-type

3.1 Plant Phenotyping

3.1.1 Hinxton Nurseries

Plant height, spike length, thousand grain weight (TGW), area, length and width of grains were measured from plants harvested from the 2023 and 2024 nursery trials in Hinxton.

Year had a significant effect ($p < 0.001$) on all traits, where the mean values for each measured trait was consistently lower in 2023 compared to 2024 (Figure 1, Table 7.) Genotype had a significant effect on plant height ($p < 0.001$), spike length ($p < 0.01$), TGW ($p < 0.01$), grain area ($p < 0.05$) and grain length ($p < 0.05$), but no effect on grain width ($p < 0.1$) (Figure 1, Table 7). The interaction between Year and Genotype also significantly affected TGW ($p < 0.05$).

In 2023, the mean *srh1* plant height was 57.2±5cm compared to 59.6±3.70 cm in the wild-type. This increased to 73.5±1.90 cm in *srh1* and 78.0±2.51 cm in the wild-type in 2024. The mean spike lengths of *srh1* and wild-type in 2023 were 7.94±0.32 cm and 8.62±0.59 cm respectively, while in 2024, mean spike lengths were 8.46±0.77 cm and 9.20±0.83 cm respectively.

TGW did not vary between the two genotypes in 2023, with both *srh1* and wild-type displaying a similar TGW value of 30.8±1.84 g and 31.0±1.54 g respectively. In contrast in 2024, mean TGW in *srh1* was 33.5±1.84 g versus 36.7±1.90 g in the wild-type. Mean grain area did not vary in 2023, with mean area values of 15.0±0.73 mm^2 in *srh1* compared to 15.2±0.47 mm^2 in the wild-type. Mean grain width between

srh1 and wild-type was similar across years, at 3.36±0.06 *mm* and 3.36±0.04 *mm* respectively for 2023, and 3.42±0.07 *mm* and 3.49±0.06 *mm* respectively for 2024. Grain length in *srh1* plants was 6.02±0.18 *mm* compared to 6.07±0.11 *mm* in wild-type plants in 2023, in contrast to 6.37±0.12 *mm* in *srh1* plants and 6.50±0.13 *mm* in wild-type plants in 2024 (Figure 1).

3.1.2 Rothamstead

Plant height, spike length, TGW and grain dimensions were measured from plants harvested from the 2024 Rothamstead trial. Genotype and generation both did not have a significant effect on any of the measured traits (Table 6).

Table 6: Summary statistics from manual plant measurements in the 2024 Rothamstead Trial.

		Sum Sq	**Mean Sq**	**NumDf**	**DenDF**	**Fvalue**	**Pr(>F)**	
Plant Height	Generation	13.079	13.079	1	12	0.4354	0.5218	
	Genotype	49.579	49.579	1	12	1.6505	0.2231	
Spike Length	Generation	0.33083	0.33083	1	12	4.215	0.06253	.
	Genotype	0.00275	0.00275	1	12	0.0351	0.85459	
TGW	Generation	0.6165	0.6165	1	12	0.1529	0.70267	
	Genotype	13.1769	13.1769	1	12	3.2669	0.09581	.
Grain Area	Generation	0.05333	0.05333	1	12	0.4599	0.5105	
	Genotype	0.4225	0.4225	1	12	3.6431	0.0805	.
Grain Length	Generation	0.003333	0.003333	1	12	0.6486	0.43626	
	Genotype	0.0225	0.0225	1	12	4.3784	0.05832	.
Grain Width	Generation	0.000833	0.000833	1	12	0.1935	0.6678	
	Genotype	0.0025	0.0025	1	12	0.5806	0.4608	
	-							
	Signif.codes:	0	’***’ 0.001	’**’ 0.01	’*’ 0.05	’.’ 0.1	’ ’ 1	

3.2 Isotope Discrimination

From flag leaves sampled on 27/6/2024, mean leaf nitrogen % (4.03±0.36)% in the *srh1* mutant was similar to that of the wild-type (4.23±0.29)%. δ15N and δ13C values in the mutant also closely resembled those of the wild-type, with mean δ15N values of 2.75±0.87 for the *srh1* mutant and 2.73±1.3 for the wild-type. Mean δ13C values were -27.4±0.98 for the mutant and -27.5±0.7 for the wild-type. Mean flag leaf carbon % was 41.2±0.92 in the mutant and 42.1±0.75 in the wild-type.

Variation in flag leaf N% was the significant between technical replicates ($p < 0.05$) across both genotypes. Flag leaf carbon % was significantly different ($p<0.05$) between the *srh1* mutant and wild-type, with the mutant displaying a lower level of carbon in dried flag leaves compared to the wild-type (Figure 2, Table 8). No significnat differences were observed between the genotypes across N%, δ15N and δ13C.

Table 7: Summary statistics from manual plant measurements in the 2023 and 2024 Hinxton Nursery Trials.

		Sum Sq	Mean Sq	NumDF	DenDF	F value	Pr(>F)		Model
Plant Height	Year	30130.6	30130.6	1	411.25	1009.141	<2.20E-16	***	∼Year * Genotype + (1 — Plot) + (1 — Block)
	Genotype	1116.4	1116.4	1	102.51	37.3903	1.78E-08	***	
	Year:Genotype	111.9	111.9	1	59.69	3.7475	0.05763	.	
Spike Length	Year	2.7515	2.7515	1	17.641	10.7063	4.32E-03	**	∼Year + Genotype + Block + (1 — Plot)
	Genotype	2.4672	2.4672	1	27.803	9.6	0.004419	**	
	Block	0.0623	0.0623	1	18.023	0.2424	0.628412		
TGW	Year	158.258	158.258	1	31.078	48.2982	8.39E-08	***	∼Year * Genotype + (1 — Block)
	Genotype	25.684	25.684	1	31.078	7.8385	0.008714	**	
	Year:Genotype	20.212	20.212	1	31.001	6.1683	0.018619	*	
Grain Area	Year	12.6698	12.6698	1	31.053	44.6378	1.78E-07	***	∼Year * Genotype + (1 — Block)
	Genotype	1.8357	1.8357	1	31.053	6.4674	0.01619	*	
	Year:Genotype	1.0932	1.0932	1	31.001	3.8517	0.05872	.	
Grain Length	Year	1.26594	1.26594	1	31.046	74.509	9.39E-10	***	∼Year * Genotype + (1 — Block)
	Genotype	0.07176	0.07176	1	31.046	4.2237	0.04836	*	
	Year:Genotype	0.01368	0.01368	1	31.001	0.8049	0.37654		
Grain Width	Year	0.077791	0.077791	1	31.139	22.9409	3.88E-05	***	∼Year * Genotype + (1 — Block)
	Genotype	0.01031	0.01031	1	31.139	3.0404	0.09108	.	
	Year:Genotype	0.009866	0.009866	1	31.002	2.9096	0.09806	.	
	Signif.codes:	0	'***' 0.001	'**' 0.01	'*' 0.05	'.' 0.1	' ' 1		

3.3 Physiology Prediction

3.3.1 Variation in Spectral Reflectance

Across all wavelengths (300nm-2500nm), significant variation was observed in mean spectral reflectance between the *srh1* mutant and wild-type plants across the 6 timepoints. Mean reflectance at 7/8/2024 (start of senescence) was most significantly different from the spectral curves of the other 5 time points, with the greatest differences observed between the wavelengths of 350nm-700nm, 770nm-1360nm, 1400nm-1850nm and 1880nm-2500nm (Figure 3).

Within each timepoint, spectral reflectance also varied significantly within each genotype. For example, at 17/8/2024, variation in spectral reflectance in the wild-type plants ranged from a minimum value of 0.426 to a maximum value of 0.529 at 1000nm (Figure 4). Median and mean values were 0.484 and 0.483 respectively with a standard error of 0.018.

Table 8: Summary statistics from flag leaf isotope discrimination

		Sum Sq	Mean Sq	NumDF	DenDF	F value	Pr(>F)	
Nitrogen%	Rep	0.06044	0.06044	1	37	4.7991	0.03485	*
	Genotype	0.02339	0.02339	1	17	1.8572	0.19073	
δ15N	Rep	0.04705	0.04705	1	37	1.7605	0.19269	
	Genotype	0.00004	0.00004	1	17	0.0014	0.97099	
Carbon%	Rep	0.00609	0.00609	1	37	0.0198	0.88888	
	Genotype	1.83507	1.83507	1	17	5.9667	0.02579	*
δ13C	Rep	0.03384	0.03384	1	37	2.2593	0.1413	
	Genotype	0.00104	0.00104	1	17	0.0692	0.79568	
	—							
	Signif. codes	: 0 '*	**' 0.00	1 '**'	0.01	'*' 0.05	'.' 0.1	' ' 1

3.3.2 Spectra QC

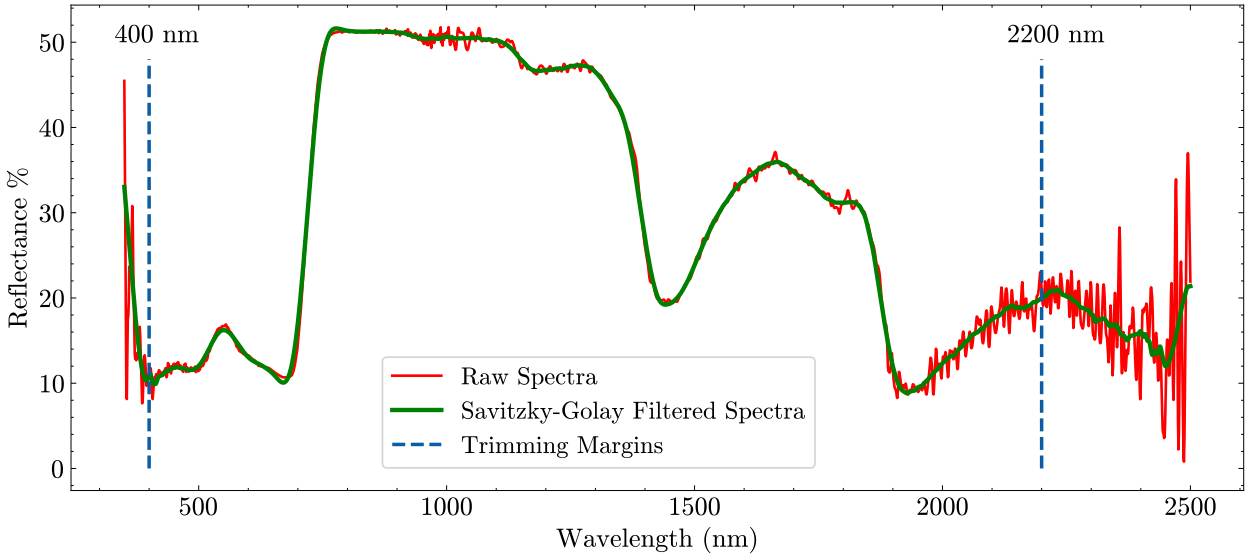

Figure 6: Example trace illustrating QC procedure for spectra obtained via the PSR+3500. Raw spectra in red, Savitzky-Golay filtered spectra in green with a window length of 100, polyorder of 2. Vertical blue dashed lines illustrate regions discarded post filtering. Wavelengths $\leq$ 400nm and $\geq$ 2200nm were discarded prior to trait prediction.

3.3.3 Predicted Traits

All 10 predicted traits (Figure 5) varied significantly ($p < 0.001$) between measurement timepoints (Table 9). Aside from V_{cmax25}/N_{area}, all other traits experienced a large drop-off in mean values at 7/8/2024 relative to mean values from the other 5 timepoints.

A significant interaction betwen Genotype and Timepoint was found in Leaf Mass Area (LMA) ($p < 0.05$)

and V_{cmax25}/N_{area} (p <0.01) (Table 9). The greatest difference in LMA between *srh1* and wild-type was during 30/7/24, where mean LMA value for the *srh1* mutant was 72.1±2.5 g/m^2 compared to 69.1±1.8 g/m^2 in the wild-type. At 7/8/24, the mean V_{cmax25}/N_{area} was greater in the wild-type (50.7±4.7 μmol CO2 s^{-1}(g N^{-1})) than *srh1* (45.2±5 μmol CO2 s^{-1}(g N^{-1})) (Figure 5).

Genotype (*srh1* and wild-type) had a significant effect on LMA (p <0.05), Leaf nitrogen area (N_{area}) (p <0.01), leaf nitrogen mass (N_{mass}) (p <0.01), SPAD (Soil Plant Analysis Development - a surrogate for chlorophyll content) (p <0.05) and stomatal conductance (Cond) (p <0.001) (Table 9).

Genotype did not have a significant effect on V_{cmax}, V_{cmax25}, J (rate of electron transport) and Photo (rate of CO_2 fixation per unit area).

3.3.4 Relationships Between Predicted Traits

LMA exhibited strong positive correlation with N_{area} (R^2 = 0.82) and SPAD (R^2 = 0.77). N_{area} was positively correlated with N_{mass} (R^2 = 0.82), although this correlation was much weaker in measurements taken during the grain forming stage (30/7/2024) (R^2 = 0.28 for *srh1* and R^2 = 0.30 for wild-type) compared to measurements during start of senescence (7/8/2024) (R^2 = 0.74 for *srh1*, R^2 = 0.79 for wild-type) (Figure 7).

J and V_{cmax25} were the two most strongly correlated traits (R^2 = 0.95), where the relationship between J and V_{cmax25} was consistent between the *srh1* mutant and wild-type, and at each timepoint. Measurements taken during the start of senescence (7/8/2024) displayed the strongest correlation between J and V_{cmax25} (R^2 = 0.94 for *srh1* and R^2 = 0.93 for wild-type) (Figure 7).

V_{cmax25}/N_{area} was negatively correlated with LMA (R^2 = -0.6), N_{area} (R^2 = -0.6) and SPAD (R^2 = -0.5) (Figure 7).

3.4 Field Scanalyzer

3.4.1 Plant Height

Across the 9 timepoints performed by the laser scanner, mean height of the *srh1* mutant was consistently shorter than the wild-type. Initial scans at 30/5/2024 indicated plant height in the mutant (14.2±3.45 *cm*) was shorter than the wild-type (18.3±5.26 *cm*). The largest difference in plant height between the genotypes occured during 19/7/2024 (Anthesis), where the *srh1* mutant was 4.81 *cm* shorter than the wild-type. The rate of height growth between each timepoint was relatively consistent between the *srh1* and wild-type.

Plant Height was statistically influenced by Genotype and Timepoint. Differences in plant height between different timepoints (p <0.001) are clearly reflected in the steady increase in plant height across the growing season in both the *srh1* mutant and wild-type (Figure 9, Table 10). Genotype had a significant effect on plant height (p <0.05, Table 10), where the *srh1* mutant was consistently shorter than the wild-type across all recorded timepoints (Figure 9). No statistical difference in the growth rate of plant height across both genotypes was detected (Table 10).

3.4.2 FVC

FVC was measured from the RGB images across 17 timepoints from May-Aug. The mean FVC of the *srh1* mutant plots were consistently lower than mean FVC of wild-type plots. Mean FVC values progressed smoothly across timepoints until reaching a maximum FVC value at 23/7/24, where mean FVC in the wild-type was 0.32±0.06 compared to 0.23±0.06 in the *srh1* mutant. Subsequent drop-off in mean FVC occured in both the *srh1* mutant and wild-type from 23/7/24 to 12/8/24.

Timepoint had a significant effect on FVC, where FVC increased consistently throughout the growth season up until 23/7/24, where FVC values subsequently decreased at 12/8/24. Genotype was not found to significantly affect FVC, and no differences in FVC growth rate were found (Table 10).

4 Discussion

4.1 Root hairs influence a multitude of traits

4.2 FVC

It is important to note that FVC does not directly account for differences in growth rates etc. FVC is affected by emergence time, tiller number. However, we have shown that there was no statistical difference in the growth rate of both plant height and FVC between the *srh1* mutant and wild-type overall, and at each specific timepoint. Tiller number different? - pending...

References

Ainsworth, Elizabeth A., Shawn P. Serbin, Jeffrey A. Skoneczka, and Philip A. Townsend (Feb. 2014). "Using leaf optical properties to detect ozone effects on foliar biochemistry". In: *Photosynthesis Research* 119.1, pp. 65–76. ISSN: 0166-8595, 1573-5079. DOI: 10.1007/s11120-013-9837-y. URL: http://link.springer.com/10.1007/s11120-013-9837-y (visited on 10/16/2024).

Barber, S. A., J. M. Walker, and E. H. Vasey (May 1963). "Mechanisms for Movement of Plant Nutrients from Soil and Fertilizer to Plant Root". In: *Journal of Agricultural and Food Chemistry* 11.3, pp. 204–207. ISSN: 0021-8561, 1520-5118. DOI: 10.1021/jf60127a017. URL: https://pubs.acs.org/doi/abs/10.1021/jf60127a017 (visited on 10/11/2024).

Bienert, Manuela Désirée, Lena M. Werner, Monika A. Wimmer, and Gerd Patrick Bienert (May 20, 2021). "Root hairs: the villi of plants". In: *Biochemical Society Transactions*, BST20200716. ISSN: 0300-5127, 1470-8752. DOI: 10.1042/BST20200716. URL: https://portlandpress.com/biochemsoctrans/article/doi/10.1042/BST20200716/228691/Root-hairs-the-villi-of-plants (visited on 10/10/2024).

Cai, Gaochao, Mutez A. Ahmed, Mohanned Abdalla, and Andrea Carminati (Mar. 2022). "Root hydraulic phenotypes impacting water uptake in drying soils". In: *Plant, Cell & Environment* 45.3, pp. 650–663. ISSN: 0140-7791, 1365-3040. DOI: 10.1111/pce.14259. URL: https://onlinelibrary.wiley.com/doi/10.1111/pce.14259 (visited on 05/18/2023).

Cai, Gaochao, Andrea Carminati, Mohanned Abdalla, and Mutez Ali Ahmed (Oct. 5, 2021). "Soil textures rather than root hairs dominate water uptake and soil–plant hydraulics under drought". In: *Plant Physiology* 187.2, pp. 858–872. ISSN: 0032-0889, 1532-2548. DOI: 10.1093/plphys/kiab271. URL: https://academic.oup.com/plphys/article/187/2/858/6297226 (visited on 10/14/2024).

Canales, Javier, Orlando Contreras-López, José M. Álvarez, and Rodrigo A. Gutiérrez (Oct. 2017). "Nitrate induction of root hair density is mediated by ¡span style="font-variant:small-caps;"¿TGA¡/span¿ 1/ ¡span style="font-variant:small-caps;"¿TGA¡/span¿ 4 and ¡span style="font-variant:small-caps;"¿CPC¡/span¿ transcription factors in *Arabidopsis thaliana*". In: *The Plant Journal* 92.2, pp. 305–316. ISSN: 0960-7412, 1365-313X. DOI: 10.1111/tpj.13656. URL: https://onlinelibrary.wiley.com/doi/10.1111/tpj.13656 (visited on 10/10/2024).

Carminati, Andrea, John B. Passioura, Mohsen Zarebanadkouki, Mutez A. Ahmed, Peter R. Ryan, Michelle Watt, and Emmanuel Delhaize (Nov. 2017). "Root hairs enable high transpiration rates in drying soils". In: *New Phytologist* 216.3, pp. 771–781. ISSN: 0028-646X, 1469-8137. DOI: 10.1111/nph.14715. URL: https://onlinelibrary.wiley.com/doi/10.1111/nph.14715 (visited on 04/11/2023).

Das, Bappa, K.K. Manohara, G.R. Mahajan, and Rabi N. Sahoo (Mar. 2020). "Spectroscopy based novel spectral indices, PCA- and PLSR-coupled machine learning models for salinity stress phenotyping of rice". In: *Spectrochimica Acta Part A: Molecular and Biomolecular Spectroscopy* 229, p. 117983. ISSN: 13861425. DOI: 10.1016/j.saa.2019.117983. URL: https://linkinghub.elsevier.com/retrieve/pii/S1386142519313824 (visited on 10/16/2024).

Datt, Bisun (Jan. 1999). "A New Reflectance Index for Remote Sensing of Chlorophyll Content in Higher Plants: Tests using Eucalyptus Leaves". In: *Journal of Plant Physiology* 154.1, pp. 30–36. ISSN: 01761617. DOI: 10.1016/S0176-1617(99)80314-9. URL: https://linkinghub.elsevier.com/retrieve/pii/S0176161799803149 (visited on 10/16/2024).

Dodd, Ian C. and Eugene Diatloff (2016). "Enhanced root growth of the brb (bald root barley) mutant in drying soil allows similar shoot physiological responses to soil water deficit as wild-type plants". In: *Functional Plant Biology* 43.2, p. 199. ISSN: 1445-4408. DOI: 10.1071/FP15303. URL: http://www.publish.csiro.au/?paper=FP15303 (visited on 04/11/2023).

Foehse, Doris and A. Jungk (Oct. 1983). "Influence of phosphate and nitrate supply on root hair formation of rape, spinach and tomato plants". In: *Plant and Soil* 74.3, pp. 359–368. ISSN: 0032-079X, 1573-5036. DOI: 10.1007/BF02181353. URL: http://link.springer.com/10.1007/BF02181353 (visited on 10/10/2024).

Fradgley, N., G. Evans, J.M. Biernaskie, J. Cockram, E.C. Marr, A. G. Oliver, E. Ober, and H. Jones (July 2020). "Effects of breeding history and crop management on the root architecture of wheat". In: *Plant and Soil* 452.1, pp. 587–600. ISSN: 0032-079X, 1573-5036. DOI: 10.1007/s11104-020-04585-2. URL: https://link.springer.com/10.1007/s11104-020-04585-2 (visited on 10/31/2022).

Furbank, Robert T., Viridiana Silva-Perez, John R. Evans, Anthony G. Condon, Gonzalo M. Estavillo, Wennan He, Saul Newman, Richard Poiré, Ashley Hall, and Zhen He (Oct. 19, 2021). "Wheat physiology predictor: predicting physiological traits in wheat from hyperspectral reflectance measurements using deep learning". In: *Plant Methods* 17.1, p. 108. ISSN: 1746-4811. DOI: 10.1186/s13007-021-00806-6. URL: https://plantmethods.biomedcentral.com/articles/10.1186/s13007-021-00806-6 (visited on 09/24/2024).

Gahoonia, Tara S. and Niels E. Nielsen (May 2004). "Barley genotypes with long root hairs sustain high grain yields in low-P field". In: *Plant and Soil* 262.1, pp. 55–62. ISSN: 0032-079X. DOI: 10.1023/B:PLSO.0000037020.58002.ac. URL: http://link.springer.com/10.1023/B:PLSO.0000037020.58002.ac (visited on 04/09/2024).

Gahoonia, Tara Singh and Niels Erik Nielsen (1998). "Direct evidence on participation of root hairs in phosphorus (32P) uptake from soil". In: *Plant and Soil* 198.2, pp. 147–152. ISSN: 0032079X. DOI: 10.1023/A:1004346412006. URL: http://link.springer.com/10.1023/A:1004346412006 (visited on 04/09/2024).

Gutierrez, Mario, Matthew P. Reynolds, and Arthur R. Klatt (July 2010). "Association of water spectral indices with plant and soil water relations in contrasting wheat genotypes". In: *Journal of Experimental Botany* 61.12, pp. 3291–3303. ISSN: 1460-2431, 0022-0957. DOI: 10.1093/jxb/erq156. URL: https://academic.oup.com/jxb/article-lookup/doi/10.1093/jxb/erq156 (visited on 10/16/2024).

Hochholdinger, Frank, Tsui-Jung Wen, Roman Zimmermann, Patricia Chimot-Marolle, Oswaldo da Costa e Silva, Wesley Bruce, Kendall R. Lamkey, Udo Wienand, and Patrick S. Schnable (June 2008). "The maize (Zea mays L.) roothairless3 gene encodes a putative GPI-anchored, monocot-specific, COBRA-like protein that significantly affects grain yield". In: *The Plant Journal* 54.5, pp. 888–898. ISSN: 0960-7412, 1365-313X. DOI: 10.1111/j.1365-313X.2008.03459.x. URL: https://onlinelibrary.wiley.com/doi/10.1111/j.1365-313X.2008.03459.x (visited on 11/16/2022).

Hunter, John D. (2007). "Matplotlib: A 2D Graphics Environment". In: *Computing in Science & Engineering* 9.3, pp. 90–95. ISSN: 1521-9615. DOI: 10.1109/MCSE.2007.55. URL: http://ieeexplore.ieee.org/document/4160265/ (visited on 09/24/2024).

Kirkham, M. B. (2014). *Principles of soil and plant water relations*. Second edition. Amsterdam ; Boston: Elsevier. 579 pp. ISBN: 978-0-12-420022-7.

Ludewig, Uwe, Nico Von Wirén, and Wolf B. Frommer (Apr. 2002). "Uniport of NH 4 + by the Root Hair Plasma Membrane Ammonium Transporter LeAMT1;1". In: *Journal of Biological Chemistry* 277.16, pp. 13548–13555. ISSN: 00219258. DOI: 10.1074/jbc.M200739200. URL: https://linkinghub.elsevier.com/retrieve/pii/S0021925819609452 (visited on 10/10/2024).

Mahajan, Gopal Ramdas, Bappa Das, Dayesh Murgaokar, Ittai Herrmann, Katja Berger, Rabi N. Sahoo, Kiran Patel, Ashwini Desai, Shaiesh Morajkar, and Rahul M. Kulkarni (Feb. 10, 2021). "Monitoring the Foliar Nutrients Status of Mango Using Spectroscopy-Based Spectral Indices and PLSR-Combined Machine Learning Models". In: *Remote Sensing* 13.4, p. 641. ISSN: 2072-4292. DOI: 10.3390/rs13040641. URL: https://www.mdpi.com/2072-4292/13/4/641 (visited on 10/16/2024).

Maqbool, Saman, Fatima Saeed, Ali Raza, Awais Rasheed, and Zhonghu He (Aug. 29, 2022). "Association of Root Hair Length and Density with Yield-Related Traits and Expression Patterns of TaRSL4 Underpinning Root Hair Length in Spring Wheat". In: *Plants* 11.17, p. 2235. ISSN: 2223-7747. DOI: 10.3390/plants11172235. URL: https://www.mdpi.com/2223-7747/11/17/2235 (visited on 10/24/2022).

Marin, M, D S Feeney, L K Brown, M Naveed, S Ruiz, N Koebernick, A G Bengough, P D Hallett, T Roose, J Puértolas, I C Dodd, and T S George (July 28, 2021). "Significance of root hairs for plant performance under contrasting field conditions and water deficit". In: *Annals of Botany* 128.1, pp. 1–16. ISSN: 0305-7364, 1095-8290. DOI: 10.1093/aob/mcaa181. URL: https://academic.oup.com/aob/article/128/1/1/5920680 (visited on 10/14/2024).

Miguel, Magalhaes Amade, Johannes Auke Postma, and Jonathan Paul Lynch (Apr. 2015). "Phene Synergism between Root Hair Length and Basal Root Growth Angle for Phosphorus Acquisition". In: *Plant Physiology* 167.4, pp. 1430–1439. ISSN: 0032-0889, 1532-2548. DOI: 10.1104/pp.15.00145. URL: https://academic.oup.com/plphys/article/167/4/1430-1439/6113693 (visited on 10/10/2024).

Montesinos-López, Osval A., Abelardo Montesinos-López, José Crossa, Gustavo De Los Campos, Gregorio Alvarado, Mondal Suchismita, Jessica Rutkoski, Lorena González-Pérez, and Juan Burgueño (Dec. 2017). "Predicting grain yield using canopy hyperspectral reflectance in wheat breeding data". In: *Plant Methods* 13.1, p. 4. ISSN: 1746-4811. DOI: 10.1186/s13007-016-0154-2. URL: http://plantmethods.biomedcentral.com/articles/10.1186/s13007-016-0154-2 (visited on 10/16/2024).

Saengwilai, Patompong, Christopher Strock, Harini Rangarajan, Joseph Chimungu, Jirawat Salungyu, and Jonathan P Lynch (Nov. 9, 2021). "Root hair phenotypes influence nitrogen acquisition in maize". In: *Annals of Botany* 128.7, pp. 849–858. ISSN: 0305-7364, 1095-8290. DOI: 10.1093/aob/mcab104. URL: https://academic.oup.com/aob/article/128/7/849/6342804 (visited on 04/11/2023).

Silva-Perez, Viridiana, Gemma Molero, Shawn P Serbin, Anthony G Condon, Matthew P Reynolds, Robert T Furbank, and John R Evans (Jan. 23, 2018). "Hyperspectral reflectance as a tool to measure biochemical and physiological traits in wheat". In: *Journal of Experimental Botany* 69.3, pp. 483–496. ISSN: 0022-0957, 1460-2431. DOI: 10.1093/jxb/erx421. URL: https://academic.oup.com/jxb/article/69/3/483/4772616 (visited on 10/16/2024).

Tsang, Ian, Jonathan A Atkinson, Stephen Rawsthorne, James Cockram, and Fiona Leigh (Sept. 27, 2024). "Root hairs: an underexplored target for sustainable cereal crop production". In: *Journal of Experimental Botany* 75.18. Ed. by Kris Vissenberg, pp. 5484–5500. ISSN: 0022-0957, 1460-2431. DOI: 10.1093/jxb/erae275. URL: https://academic.oup.com/jxb/article/75/18/5484/7696010 (visited on 10/11/2024).

Yang, Na, Changhua Zhu, Lijun Gan, Denny Ng, and Kai Xia (Apr. 2011). "Ammonium-Stimulated Root Hair Branching is Enhanced by Methyl Jasmonate and Suppressed by Ethylene in Arabidopsis thaliana". In: *Journal of Plant Biology* 54.2, pp. 92–100. ISSN: 1226-9239, 1867-0725. DOI: 10.1007/s12374-011-9147-x. URL: http://link.springer.com/10.1007/s12374-011-9147-x (visited on 10/10/2024).

Yao, Xia, Yu Huang, Guiyan Shang, Chen Zhou, Tao Cheng, Yongchao Tian, Weixing Cao, and Yan Zhu (Nov. 10, 2015). "Evaluation of Six Algorithms to Monitor Wheat Leaf Nitrogen Concentration". In: *Remote Sensing* 7.11, pp. 14939–14966. ISSN: 2072-4292. DOI: 10.3390/rs71114939. URL: https://www.mdpi.com/2072-4292/7/11/14939 (visited on 10/16/2024).

Yendrek, Craig R., Tiago Tomaz, Christopher M. Montes, Youyuan Cao, Alison M. Morse, Patrick J. Brown, Lauren M. McIntyre, Andrew D.B. Leakey, and Elizabeth A. Ainsworth (Jan. 2017). "High-Throughput Phenotyping of Maize Leaf Physiological and Biochemical Traits Using Hyperspectral Reflectance". In: *Plant Physiology* 173.1, pp. 614–626. ISSN: 0032-0889, 1532-2548. DOI: 10.1104/pp.16.01447. URL: https://academic.oup.com/plphys/article/173/1/614-626/6116016 (visited on 10/16/2024).

Zhu, Jinming, Chaochun Zhang, and Jonathan P. Lynch (2010). "The utility of phenotypic plasticity of root hair length for phosphorus acquisition". In: *Functional Plant Biology* 37.4, p. 313. ISSN: 1445-4408. DOI: 10.1071/FP09197. URL: http://www.publish.csiro.au/?paper=FP09197 (visited on 10/10/2024).

Zhu, Lingxiao, Liantao Liu, Hongchun Sun, Yongjiang Zhang, Xiuwei Liu, Nan Wang, Jing Chen, Ke Zhang, Zhiying Bai, Guiyan Wang, Liwen Tian, and Cundong Li (Feb. 2022). "The responses of lateral roots and root hairs to nitrogen stress in cotton based on daily root measurements". In: *Journal of Agronomy*

and Crop Science 208.1, pp. 89–105. ISSN: 0931-2250, 1439-037X. DOI: 10.1111/jac.12525. URL: https://onlinelibrary.wiley.com/doi/10.1111/jac.12525 (visited on 10/10/2024).

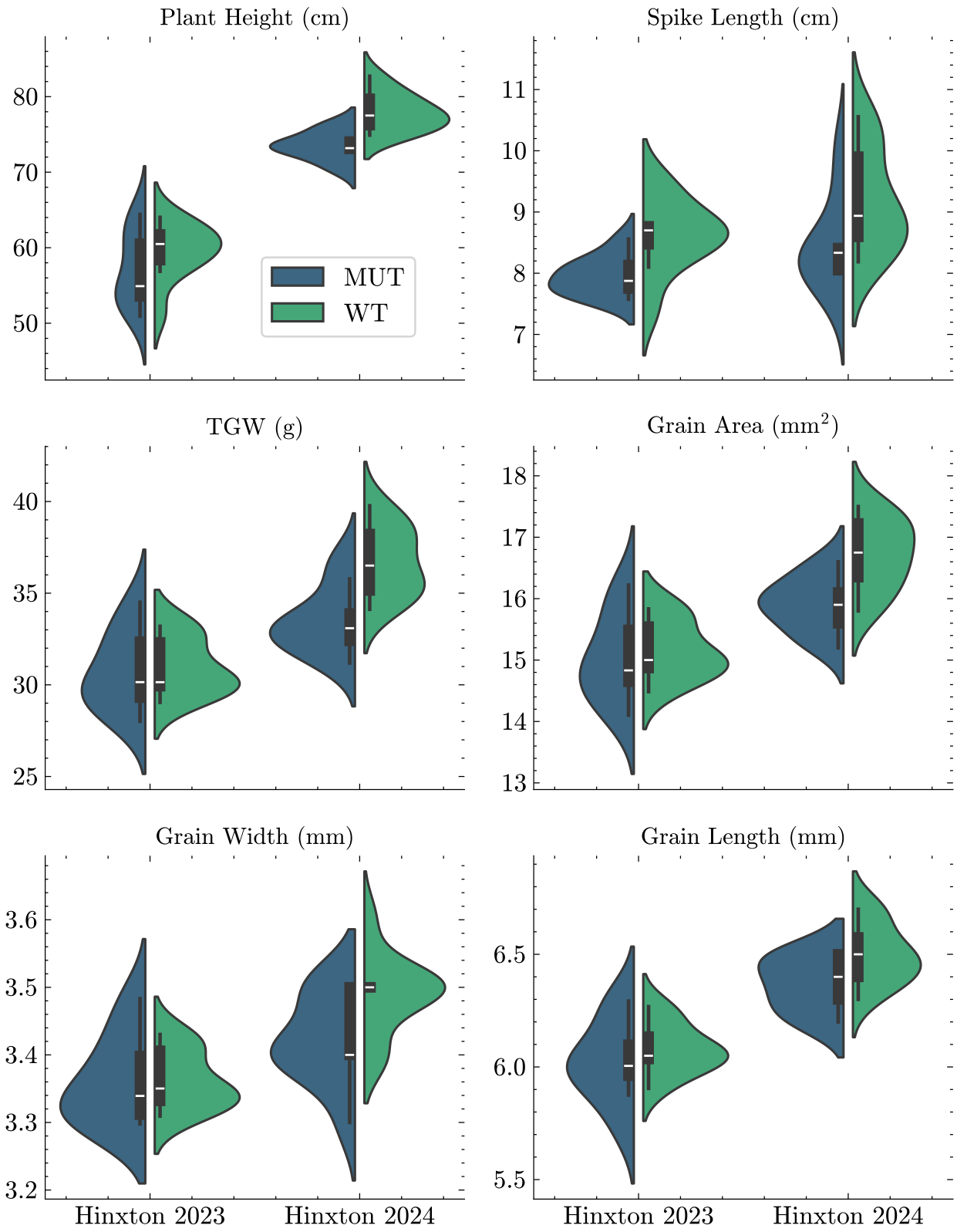

Figure 1: Physiological traits of the *srh1* mutant and wild-type plants in 2023 and 2024 Hinxton Nurseries.

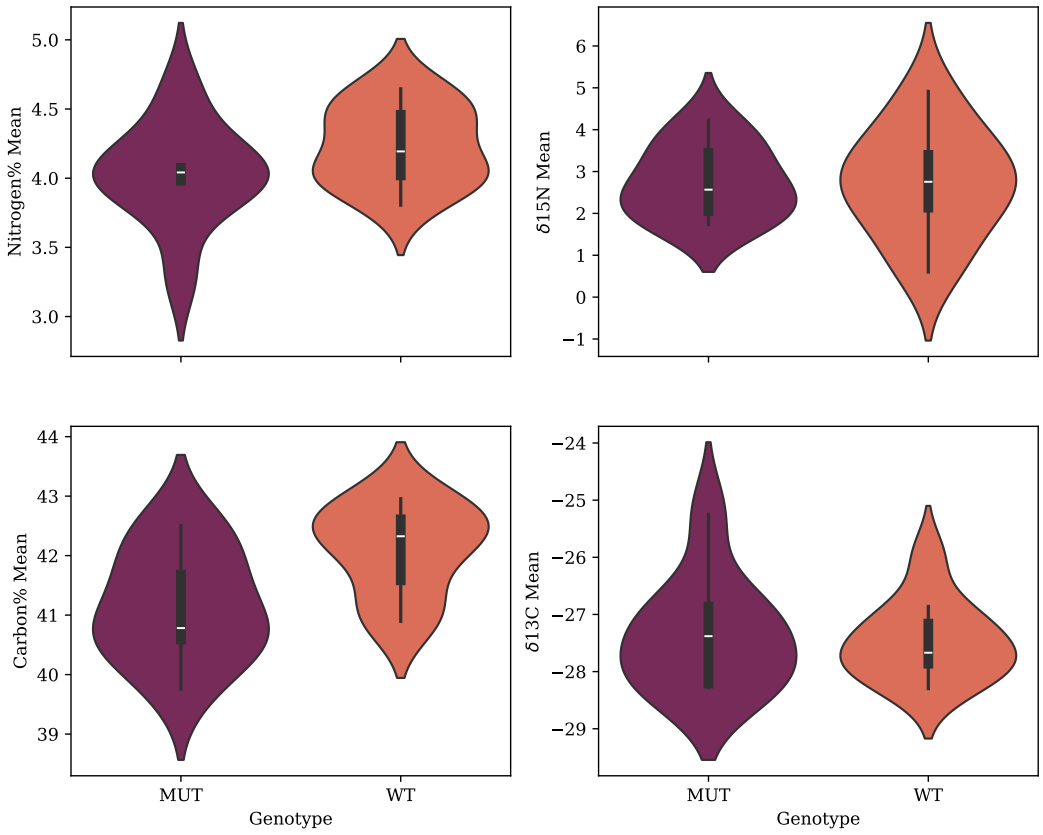

Figure 2: Isotope discrimination from flag leaf discs (harvested 27/6/24) of the *srh1* mutant and wild-type plants grown in the 2024 nursery trial, measured via mass spectrometry.

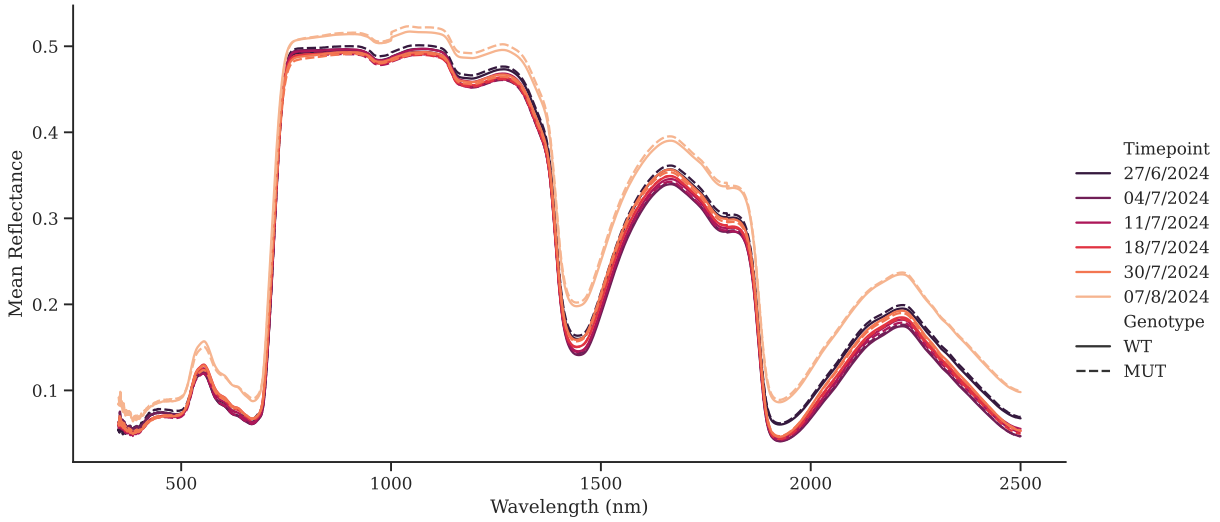

Figure 3: Mean spectral reflectance from flag leaves of the *srh1* mutant and wild-type grown in the field in 2024. Colours represent mean reflctance from different measurement time points; solid lines indicate *srh1*, dashed lines indicate wild-type.

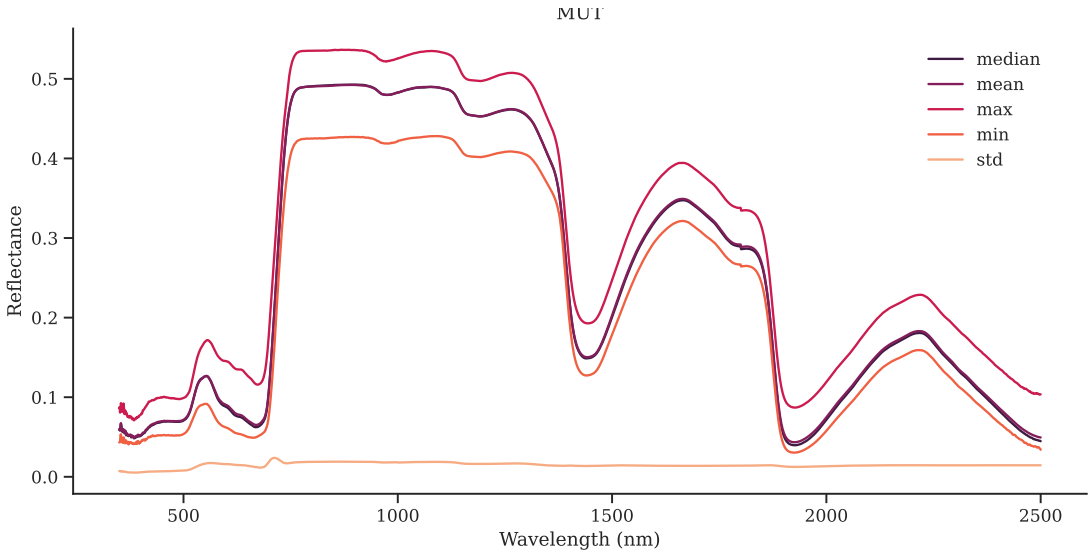

Figure 4: Variation in spectral reflectance in wild-type leaves at 18/7/24 (Flowering/Anthesis).

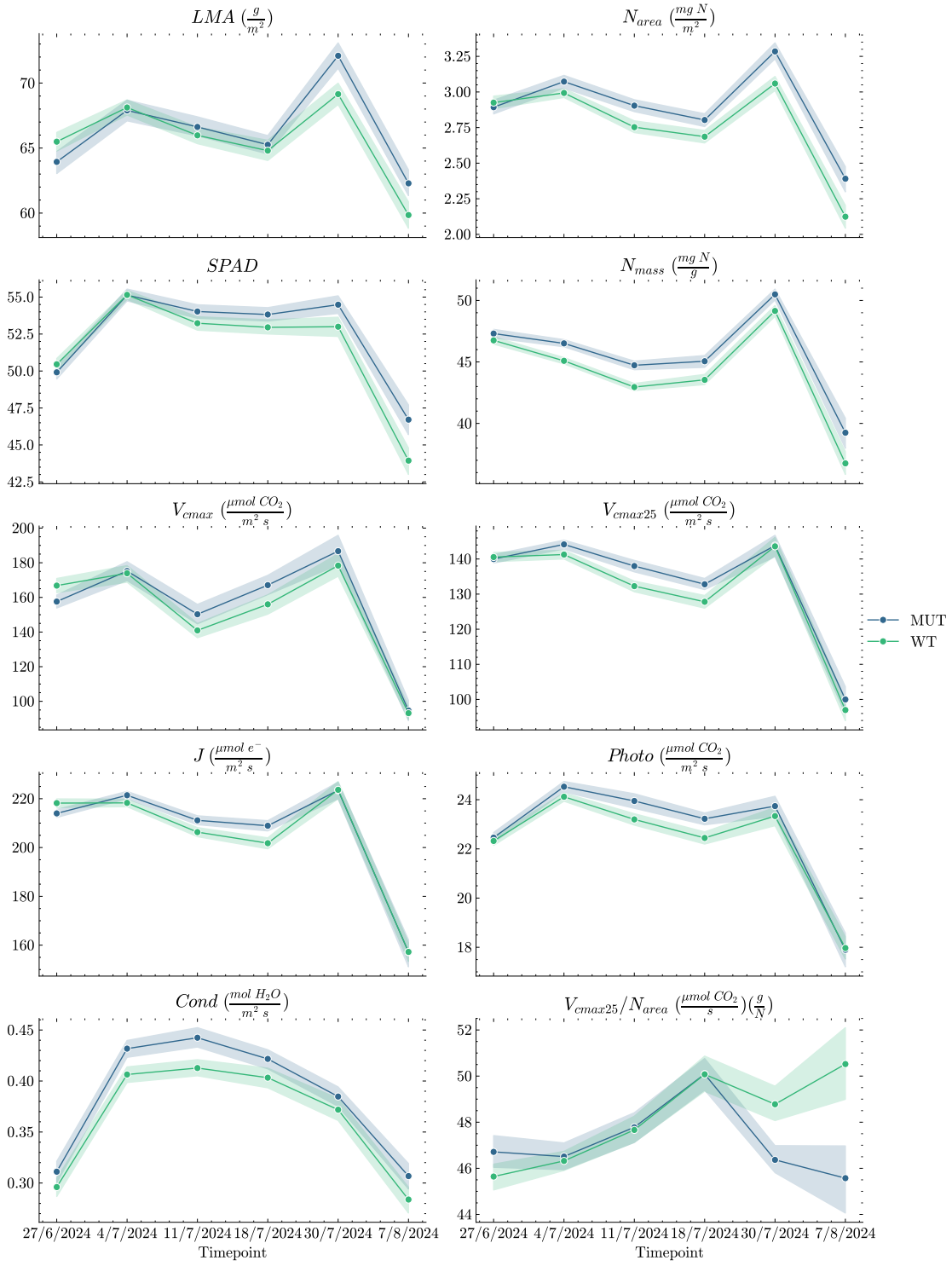

Figure 5: Physiology traits predicted using Wheat Physiology Predictor (Furbank et al. 2021) from raw spectral reflectance data. Solid lines illustrate mean values across all plots for each gneotype, bands indicate range of data.

Table 9: Summary statistics for predicted traits from spectral reflectance data

		Sum Sq	**Mean Sq**	**NumDF**	**DenDF**	**F value**	**Pr(>F)**	
LMA	Genotype	9	9.5	1	17	1.9211	0.183646	
	Timepoint	975	195	5	85	39.4359	<2.2e-16	***
	Genotype:Timepoint	70	14.1	5	85	2.851	0.019853	*
N_{area}	Genotype	0	0.4	1	17	12.3942	0.002625	**
	Timepoint	10	1.9	5	85	65.6896	<2.2e-16	***
	Genotype:Timepoint	0	0	5	85	1.6759	0.149182	
SPAD	Genotype	19	18.8	1	17	5.2994	0.034247	*
	Timepoint	1257	251.4	5	85	70.9054	<2.2e-16	***
	Genotype:Timepoint	29	5.9	5	85	1.6518	0.15518	
N_{mass}	Genotype	34	34.1	1	17	11.2546	0.003758	**
	Timepoint	1566	313.3	5	85	103.2761	<2.2e-16	***
	Genotype:Timepoint	7	1.3	5	85	0.4388	0.820228	
V_{cmax}	Genotype	241	241.1	1	17	1.3253	0.265583	
	Timepoint	98756	19751.2	5	85	108.5845	<2.2e-16	***
	Genotype:Timepoint	1384	276.7	5	85	1.5214	0.19174	
V_{cmax25}	Genotype	122	122	1	17	3.3062	0.086685	.
	Timepoint	28865	5772.9	5	85	156.4416	<2.2e-16	***
	Genotype:Timepoint	163	32.6	5	85	0.8839	0.49563	
J	Genotype	37	37.3	1	17	0.5287	0.477066	
	Timepoint	59094	11818.8	5	85	167.6234	<2.2e-16	***
	Genotype:Timepoint	467	93.5	5	85	1.3259	0.260994	
Photo	Genotype	2	2.3	1	17	2.2144	0.155039	
	Timepoint	525	105.1	5	85	100.984	<2.2e-16	***
	Genotype:Timepoint	5	1	5	85	0.9334	0.463637	
Cond	Genotype	0	0	1	102	16.0437	0.000118	***
	Timepoint	0	0.1	5	102	88.4021	<2.2e-16	***
	Genotype:Timepoint	0	0	5	102	0.2263	0.950356	
V_{cmax25}/N_{area}	Genotype	22	22	1	17	3.484	0.079312	.
	Timepoint	186	37.2	5	85	5.879	0.000103	***
	Genotype:Timepoint	140	28	5	85	4.4251	0.001248	**
	—							
	Signif. codes:	'***' 0.001	'**' 0.01	1	'*' 0.05 '	.' 0.1 '	' 1	

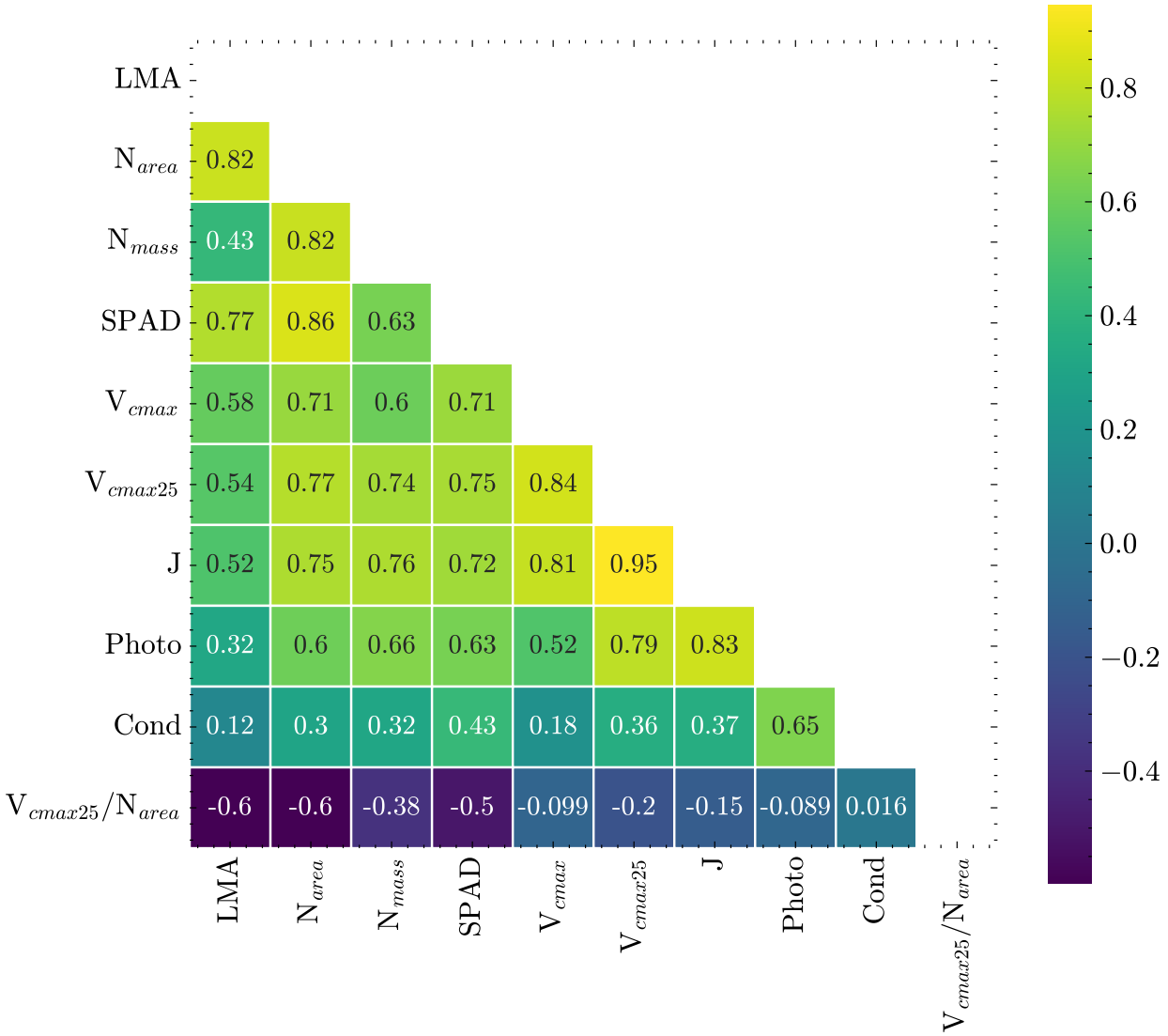

Figure 7: Correlation matrix illustrating relationships between the ten predicted traits for both genotypes across all timepoints.

Table 10: Summary statistics for plant height, height growth rate, FVC and FVC growth rate between the *srh1* mutant and wild-type.

		SumSq	**MeanSq**	**NumDF**	**DenDF**	**F value**	**Pr(>F)**	
Plant Height	Generation	2	1.7	1	12	0.2766	0.6085	
	Timepoint	45229	5653.7	8	120	912.2813	<2e-16	***
	Genotype	32	31.8	1	12	5.1254	0.0429	*
FVC	Generation	0.00003	0.000033	1	12	0.0455	0.83466	
	Timepoint	1.84274	0.115171	16	240	158.9563	<2e-16	***
	Genotype	0.00273	0.002734	1	12	3.7728	0.07593	.
Plant Height Rate	Generation	0	0	1		0.0002	0.99	
	Timepoint	49.424	6.1781	8		56.0903	<2e-16	***
	Genotype	0.004	0.0045	1		0.0406	0.8406	
	Residuals	14.649	0.1101	133				
FVC Rate	Generation	4.2E-06	4.19E-06	1		0.179	0.6726	
	Timepoint	0.008223	0.000514	16		21.9806	<2e-16	***
	Genotype	5.8E-06	5.76E-06	1		0.2464	0.62	
	Residuals	0.005892	2.34E-05	252				
	-							
	Signif.codes:	0	'***' 0.001	'**' 0.01	'*' 0.05	'.' 0.1	' ' 1	

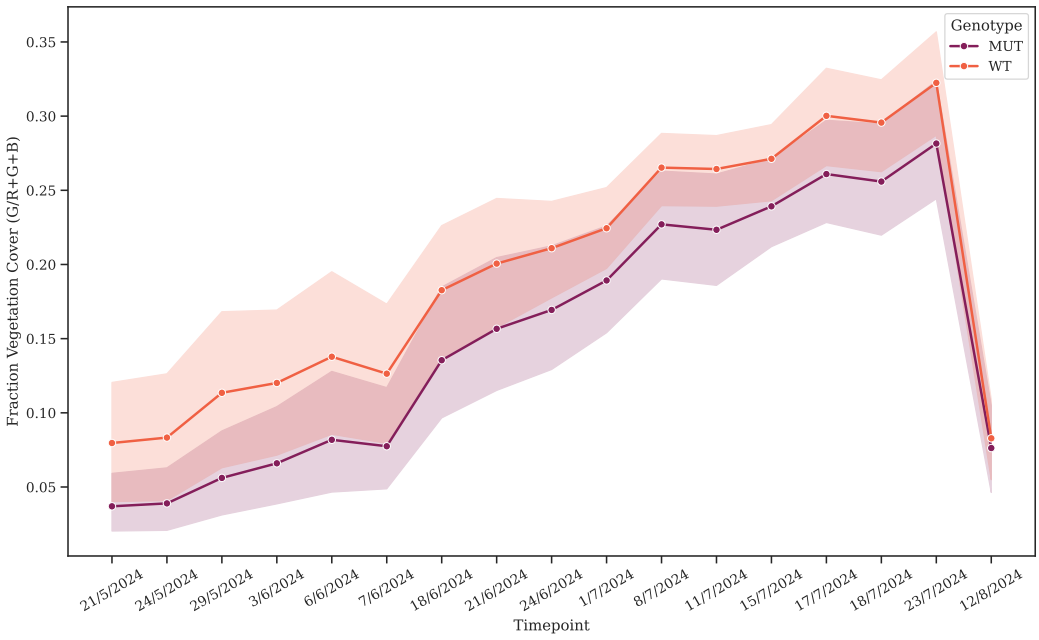

Figure 8: Fraction Vegetation Cover (FVC) in the *srh1* mutant and wild-type from emergence till senescence, grown at Rothamstead Research in 2024. FVC was calculated from RGB images taken by the Field Scanalyzer. FVC is expressed as a ratio of green pixels to total pixels. Solid line illustrates mean FVC for each timepoint, bands illustrate range.

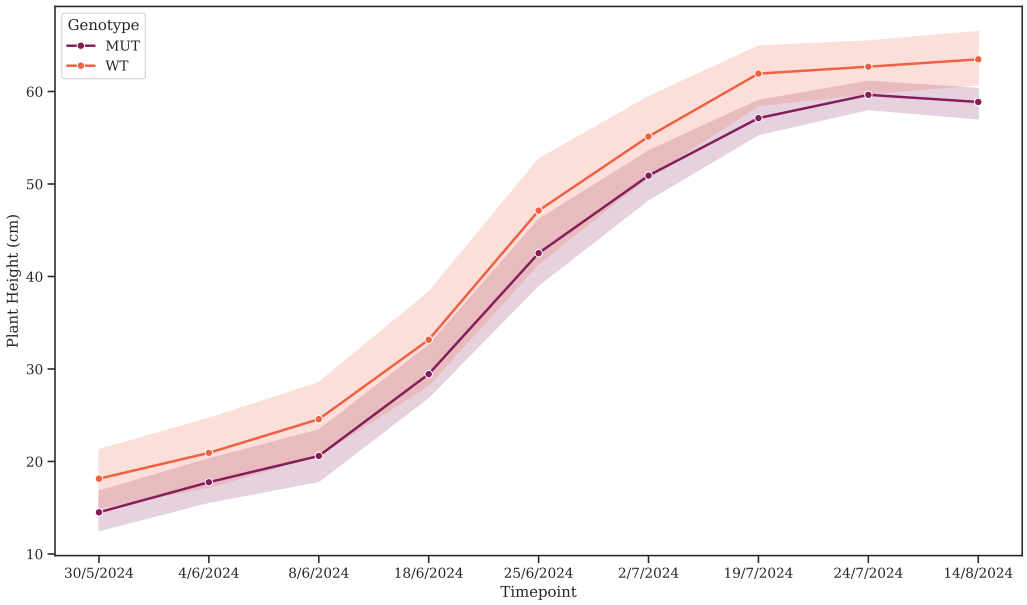

Figure 9: Plant Height (cm) of the *srh1* mutant and wild-type grown at Rothamstead Research in 2024. Plant Height was calculated from 3D point clouds of each plot via the laser scanner on the Field Scanalyzer. Solid line illustrates mean plant height for each timepoint, bands illustrate range.